

## Supporting Information

Jiao Meng,<sup>1,2</sup> Yue Zhao,<sup>1,2</sup> Haining Li,<sup>3</sup> Ruiping Chen,<sup>4</sup> Xun Sun,<sup>\*1,2</sup> Xuan Sun<sup>\*3</sup>

<sup>1</sup>State Key Laboratory of Crystal Materials, Shandong University, Jinan 250100, China. Email:sunxun@sdu.edu.cn

<sup>2</sup>Key Laboratory of Functional Crystal Materials and Device, Shandong University, Ministry of Education, Jinan, 250100, P. R. China. Email:sunxun@sdu.edu.cn

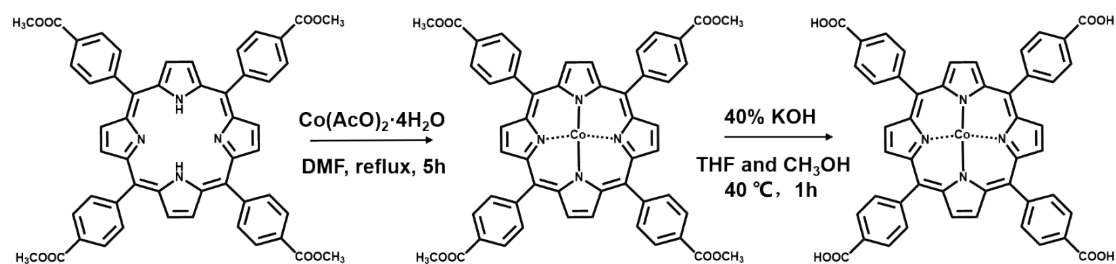
<sup>3</sup>Key Laboratory of Colloid and Interface Chemistry, Ministry of Education, School of Chemistry and Chemical Engineering, Shandong University, Jinan 250100, P. R.China. E-mail: sunxuan@sdu.edu.cn

<sup>4</sup>State Key Lab of Structural Chemistry Fujian Institute of Research on the Structure of Matter, Chinese Academy of Sciences Fuzhou, 350002 (P.R. China)

### Contents

<b>1. Figures</b>	<b>2</b>
<b>2. Tables</b>	<b>13</b>

## Figures



**Scheme S1** The synthesis of cobalt 5, 10, 15, 20 - meso - tetra (4-carboxyphenyl) porphyrin.

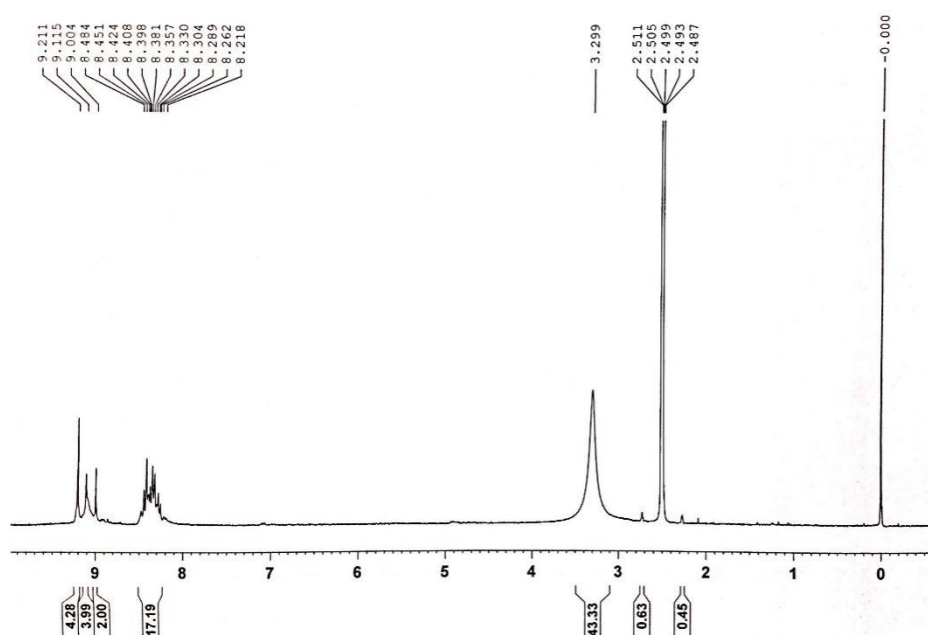


**Fig. S1**  $^1\text{H}$  NMR spectra of CoTCPP monomer.

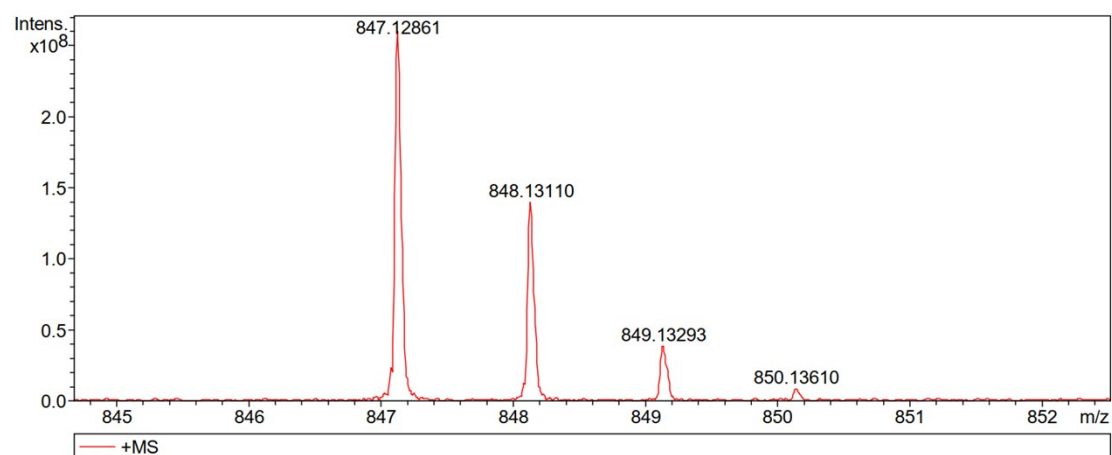


**Fig. S2** HRMS spectrum of CoTCPP monomer dissolved in  $\text{CH}_3\text{OH}$ .

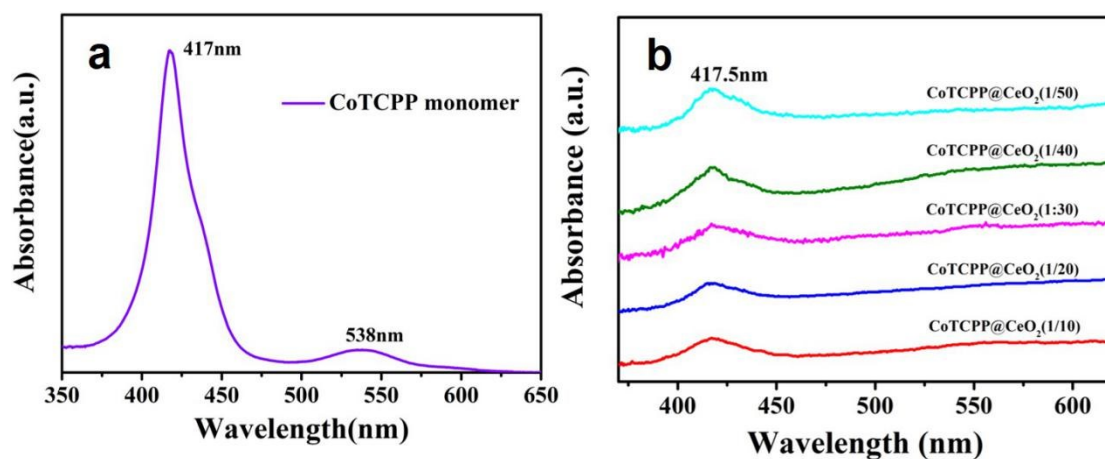


**Fig. S3** Ultraviolet visible absorption spectrum of (a) CoTCPP monomer and (b) CoTCPP@CeO<sub>2</sub>.

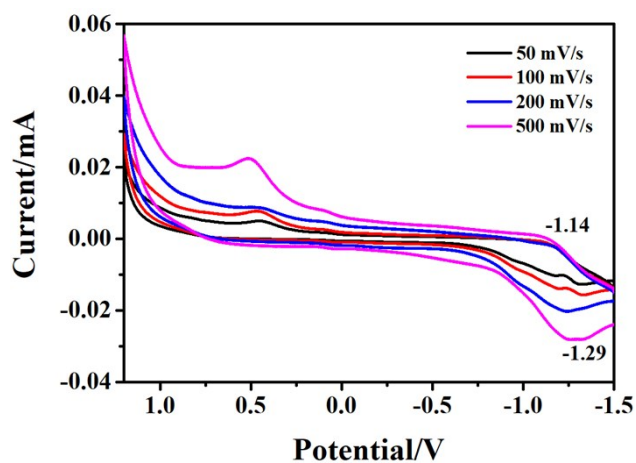


**Fig. S4** Cyclic voltammetry curves of CoTCPP monomer at different sweep speeds, the samples were dissolved in DMF.

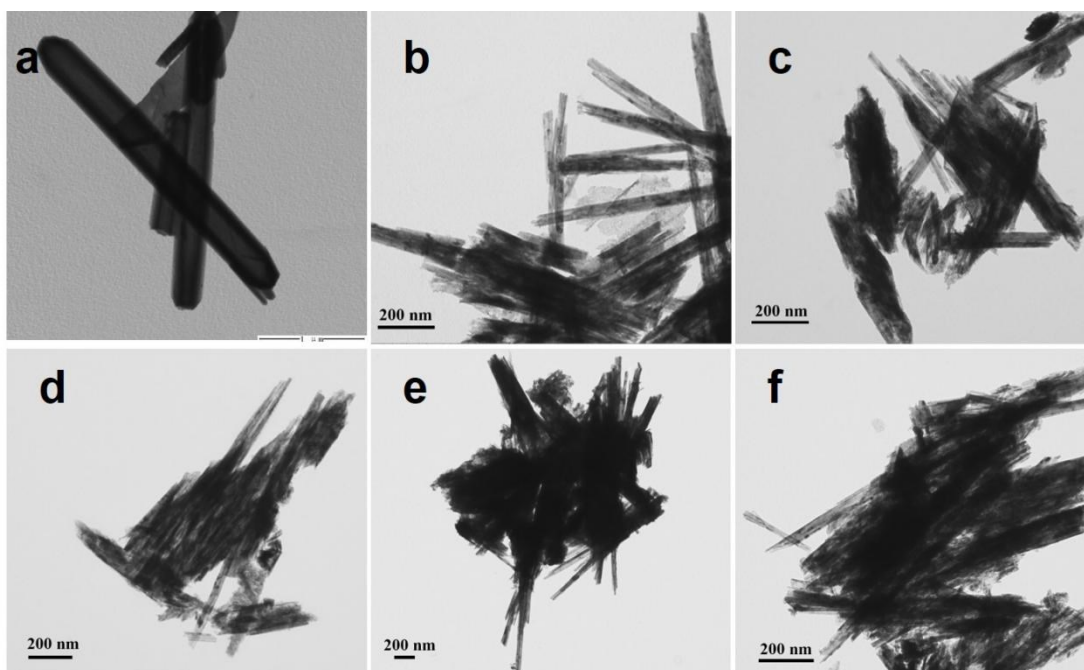


**Fig. S5** TEM images of ceria hollow nanorods (a), composite materials in different mass ratio ( $\text{CoTCPP@CeO}_2$ ) (b) 1/10, (c) 1/20, (d) 1/30, (e) 1/40, (f) 1/50, just synthesized.

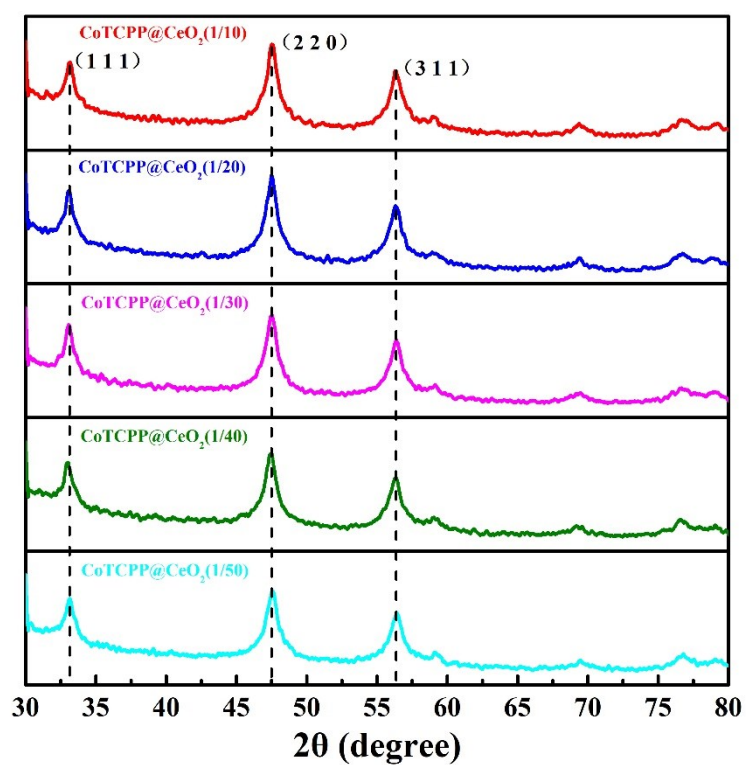


**Figure S6** XRD patterns of a series of  $\text{CoTCPP@CeO}_2$ .

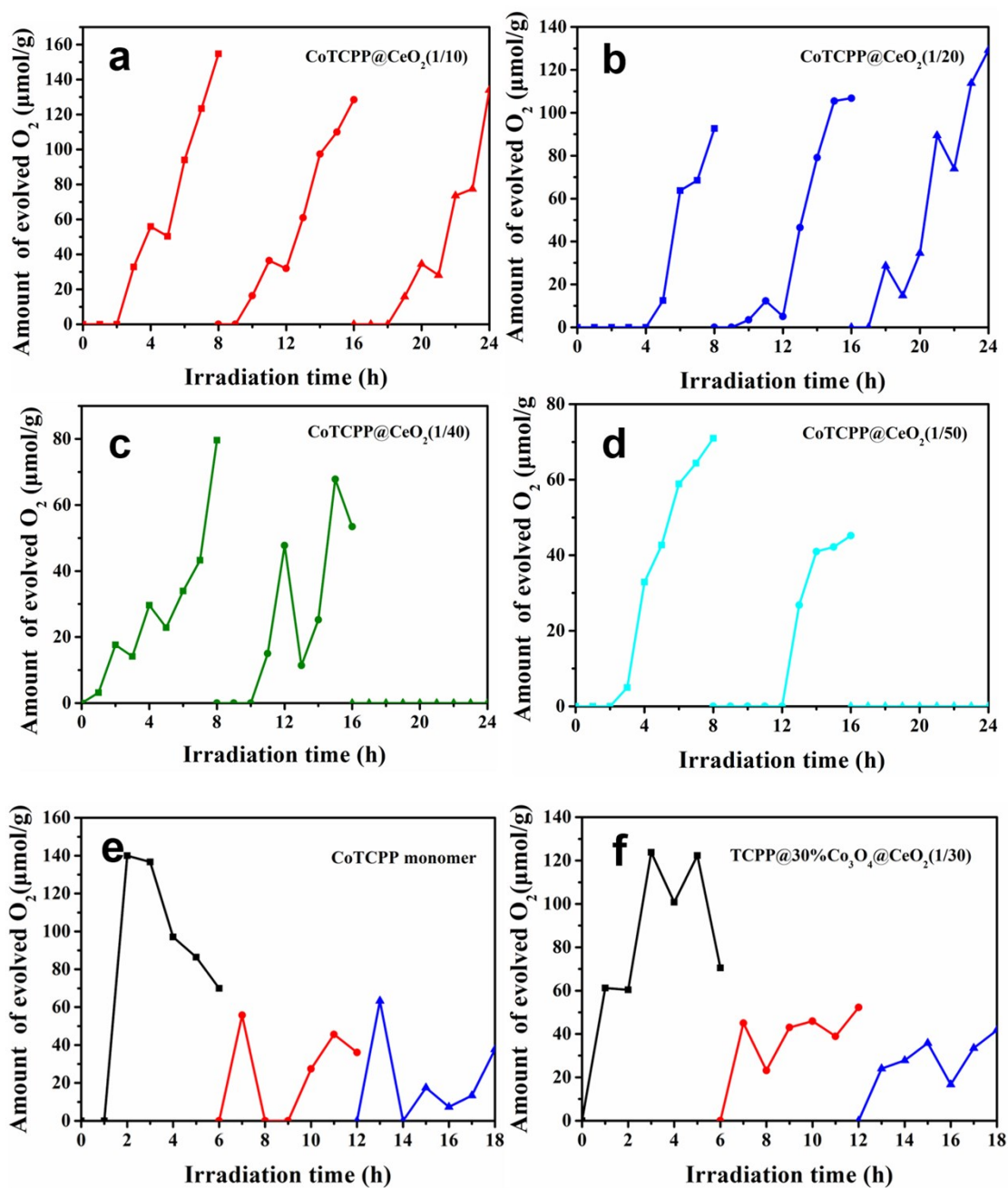


**Fig. S7** Cyclic oxygen production of the (a) CoTCPP@CeO<sub>2</sub> (1/10), (b) CoTCPP@CeO<sub>2</sub> (1/20), (c) CoTCPP@CeO<sub>2</sub> (1/40), (d) CoTCPP@CeO<sub>2</sub> (1/50), (e) CoTCPP monomer and (f) TCPP@30%Co<sub>3</sub>O<sub>4</sub>@CeO<sub>2</sub> (1/30).

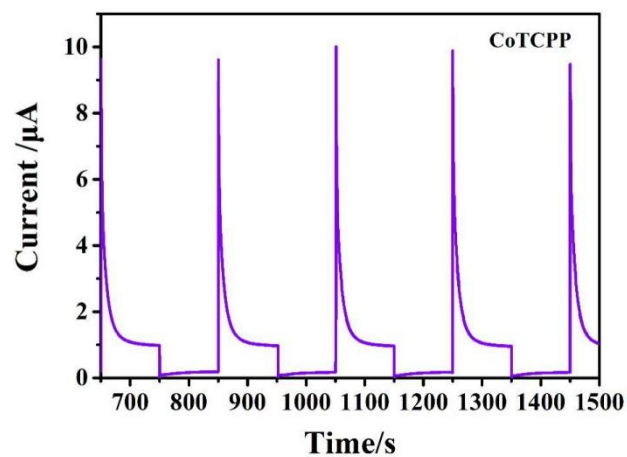


Fig. S8 Transient photocurrent response of the CoTCPP monomer.

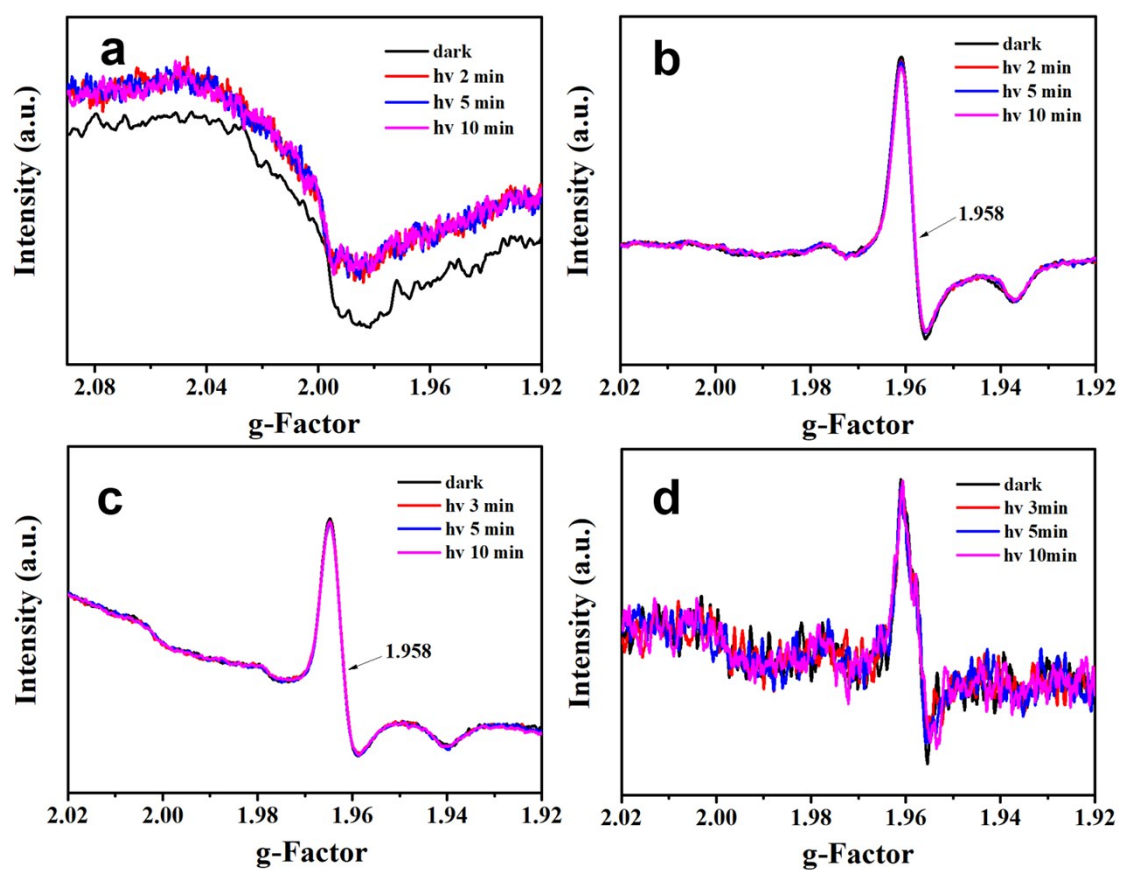
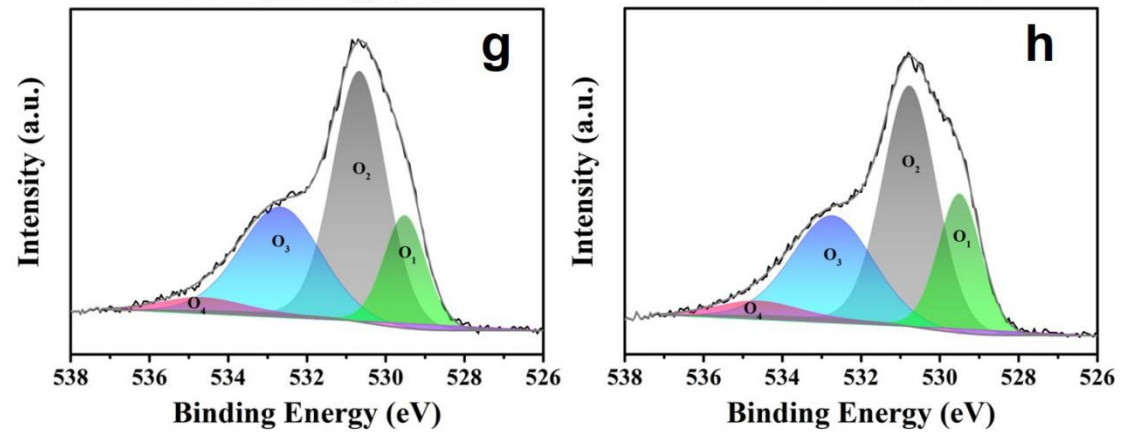
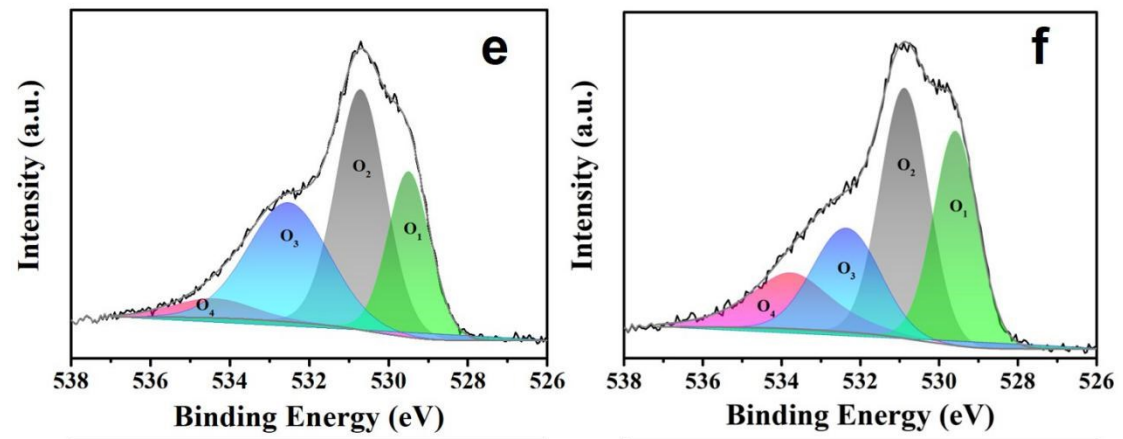
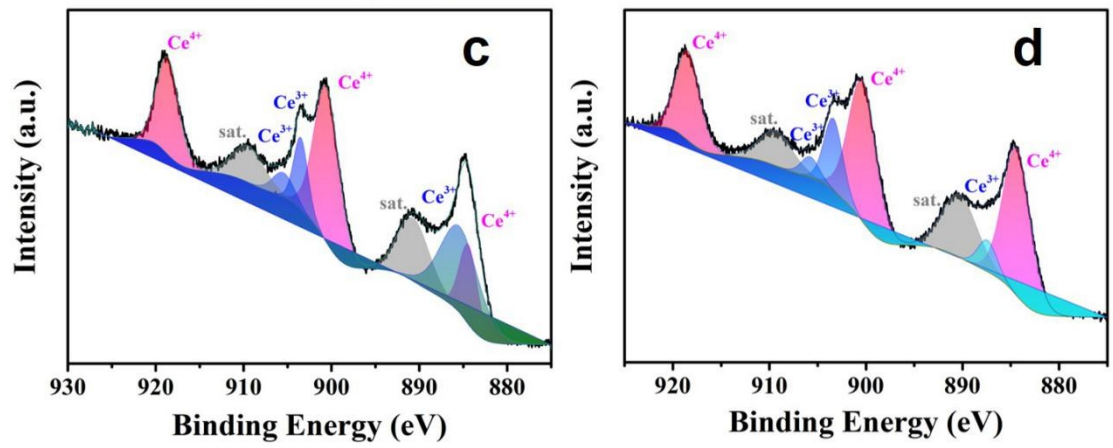
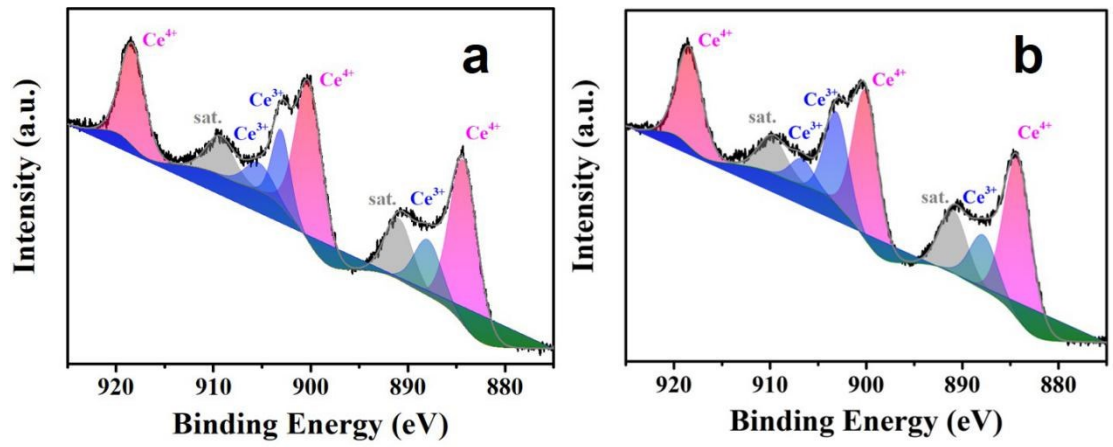
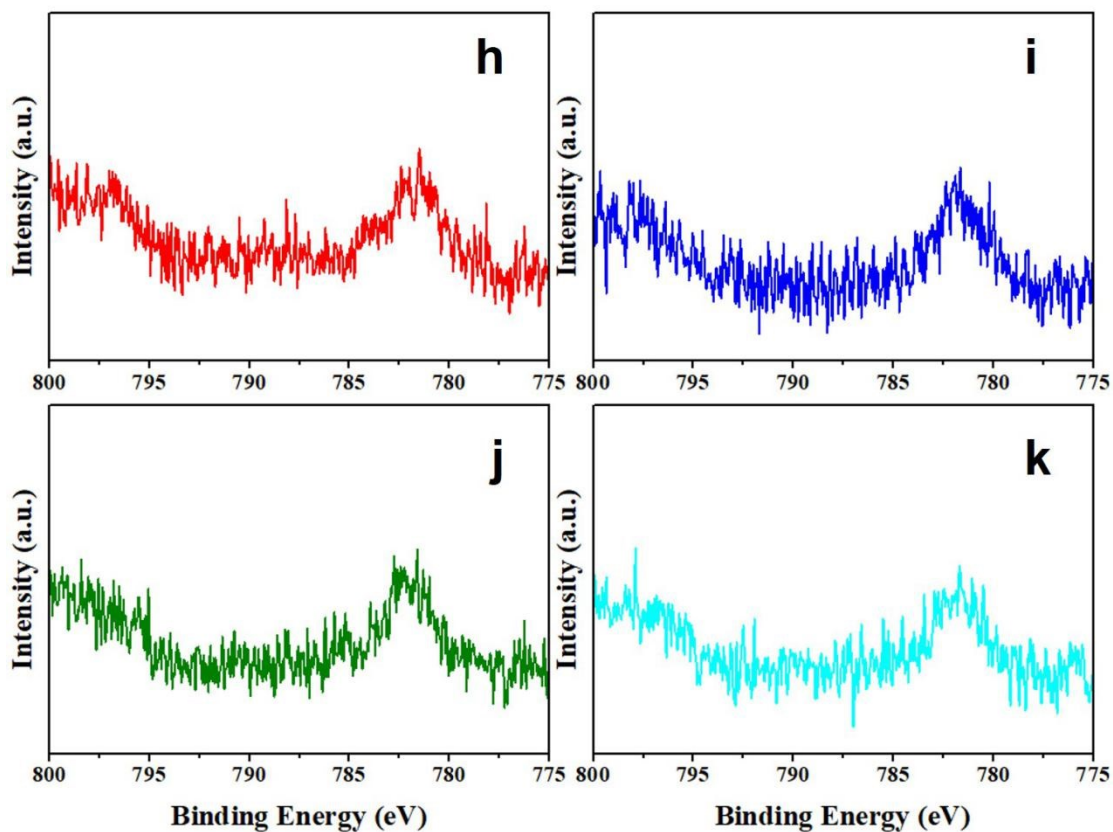
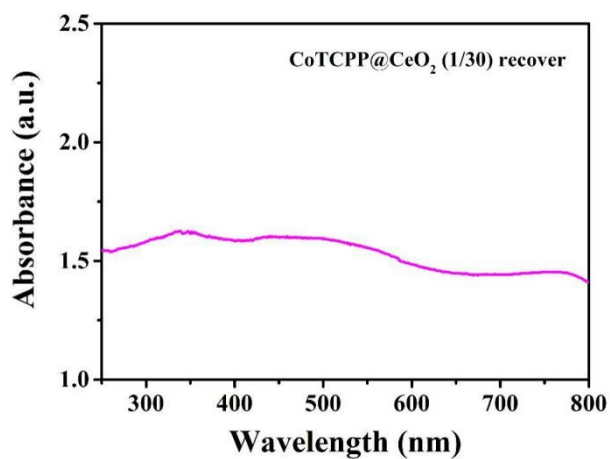


Fig. S9 EPR signal of the (a) CoTCPP monomer, (b)  $\text{CeO}_2$ , (c)  $\text{TCPP}@30\%\text{Co}_3\text{O}_4@\text{CeO}_2$  (1/30) and (d)  $30\%\text{Co}_3\text{O}_4@\text{CeO}_2$ .





**Fig. S10** Ce 3d XPS spectra (a, b, c, d), O 1s XPS spectra (e, f, g, h) and Co 2p XPS spectra (h, i, j, k) of CoTCPP@CeO<sub>2</sub> (1/10) (a, e, h), CoTCPP@CeO<sub>2</sub> (1/20) (b, f, i), CoTCPP@CeO<sub>2</sub> (1/40) (c, g, j) and CoTCPP@CeO<sub>2</sub> (1/50) (d, h, k), respectively.



**Fig. S11** Absorption spectra of the CoTCPP@CeO<sub>2</sub> (1/30) after the OER.



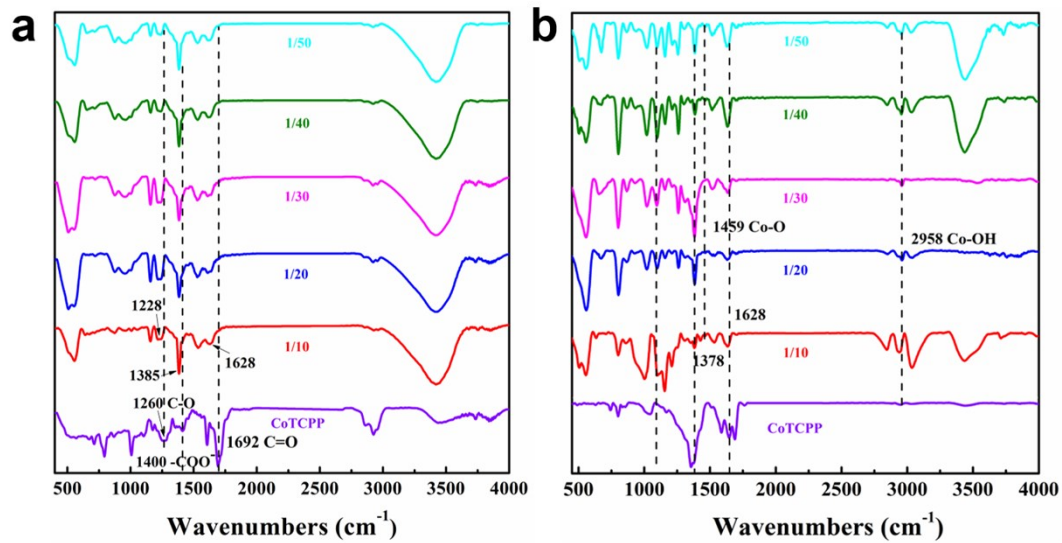


Fig. S12 Fourier transform infrared spectroscopy (FTIR) of a series of  $\text{CoTCPP@CeO}_2$ .

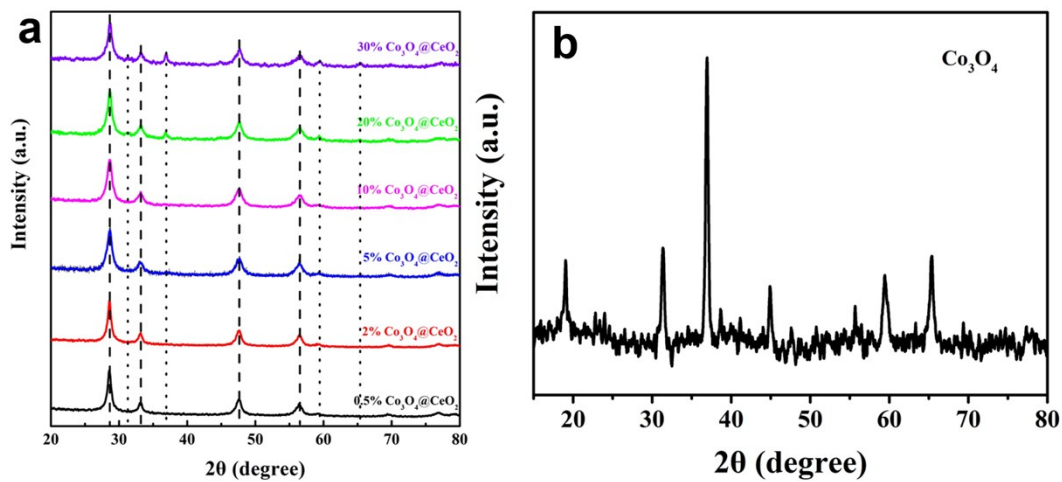
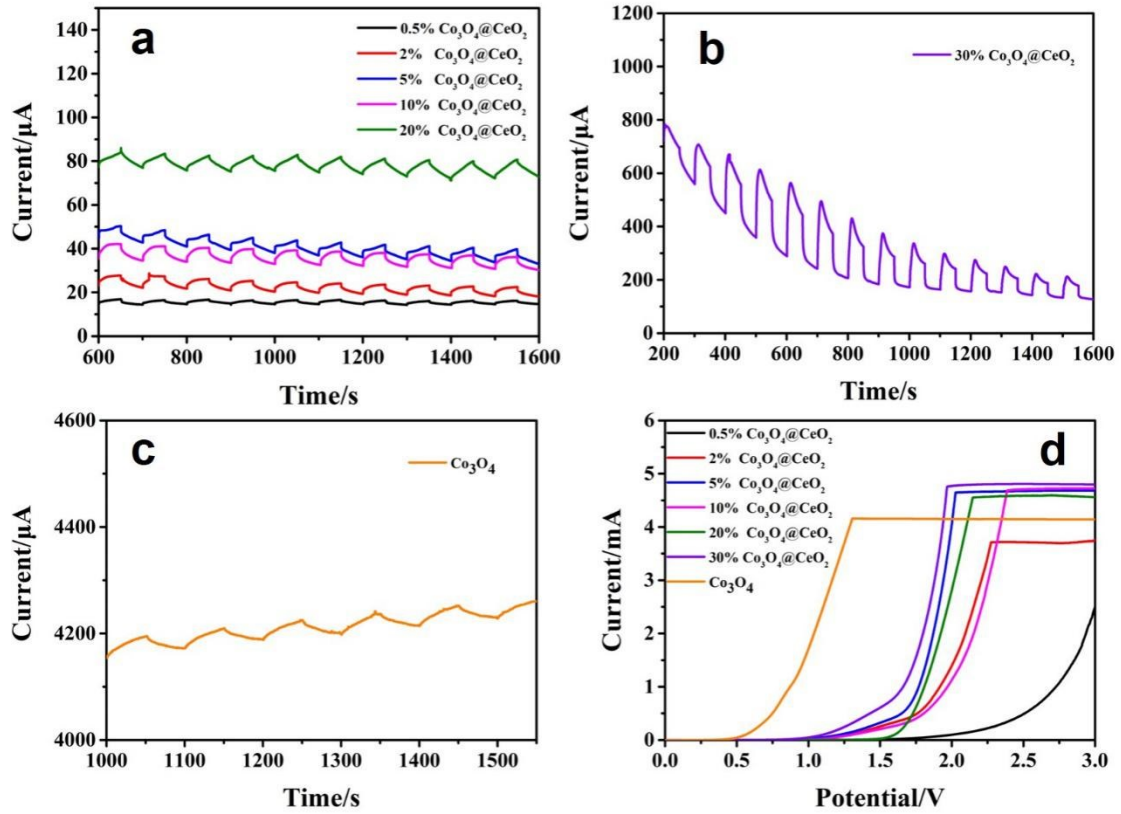
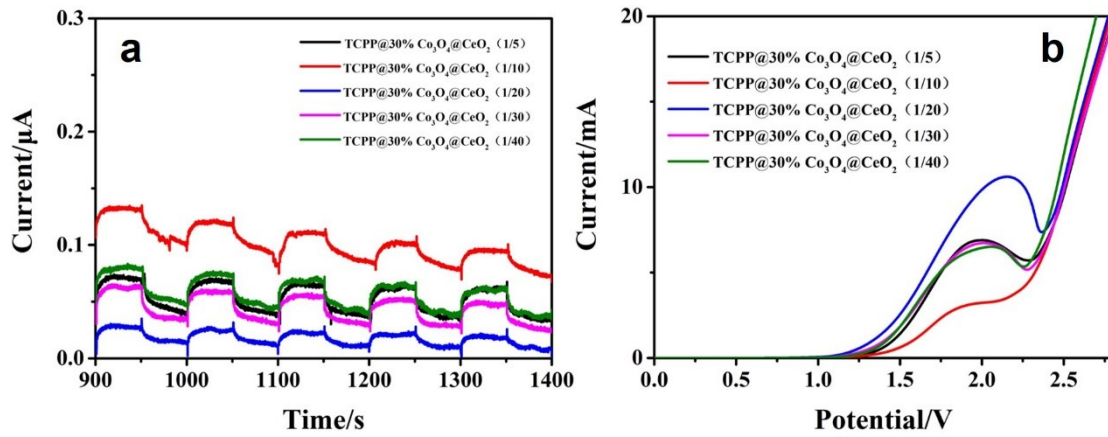


Fig.

S13 XRD patterns of the  $\text{Co}_3\text{O}_4@\text{CeO}_2$  NTs and the pure  $\text{Co}_3\text{O}_4$ . (The characteristic peaks of  $\text{CeO}_2$  are marked by dash line and  $\text{Co}_3\text{O}_4$  by dot line.)  $\text{CeO}_2$  (1 1 1) (2 0 0) (2 2 0) (3 1 1) ;  $\text{Co}_3\text{O}_4$  (2 2 0) (3 1 1) (5 1 1) (4 4 0)



**Fig. S14** (a) (b) Transient photocurrent response of the  $\text{Co}_3\text{O}_4@\text{CeO}_2$  in different cobalt oxide content and (c) the pure  $\text{Co}_3\text{O}_4$ ; (d) overpotential test of a series of  $\text{Co}_3\text{O}_4@\text{CeO}_2$ .



**Fig. S15** (a) Transient photocurrent response of the TCPP@30% $\text{Co}_3\text{O}_4@\text{CeO}_2$  in different TCPP content and (d) overpotential test of a series of TCPP@30% $\text{Co}_3\text{O}_4@\text{CeO}_2$ .

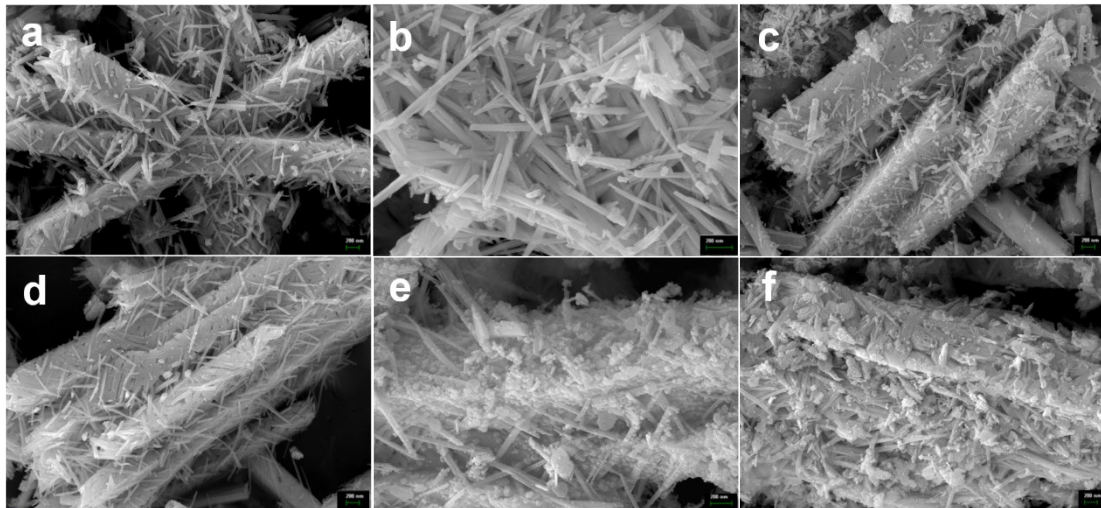


**Fig. S16** SEM images of the  $\text{Co}_3\text{O}_4@\text{CeO}_2$ , composite materials with different  $\text{Co}_3\text{O}_4$  content (a) 0.5%, (b) 10%, (c) 20%, (d) 30%, (e) 40%, (f) 50%.

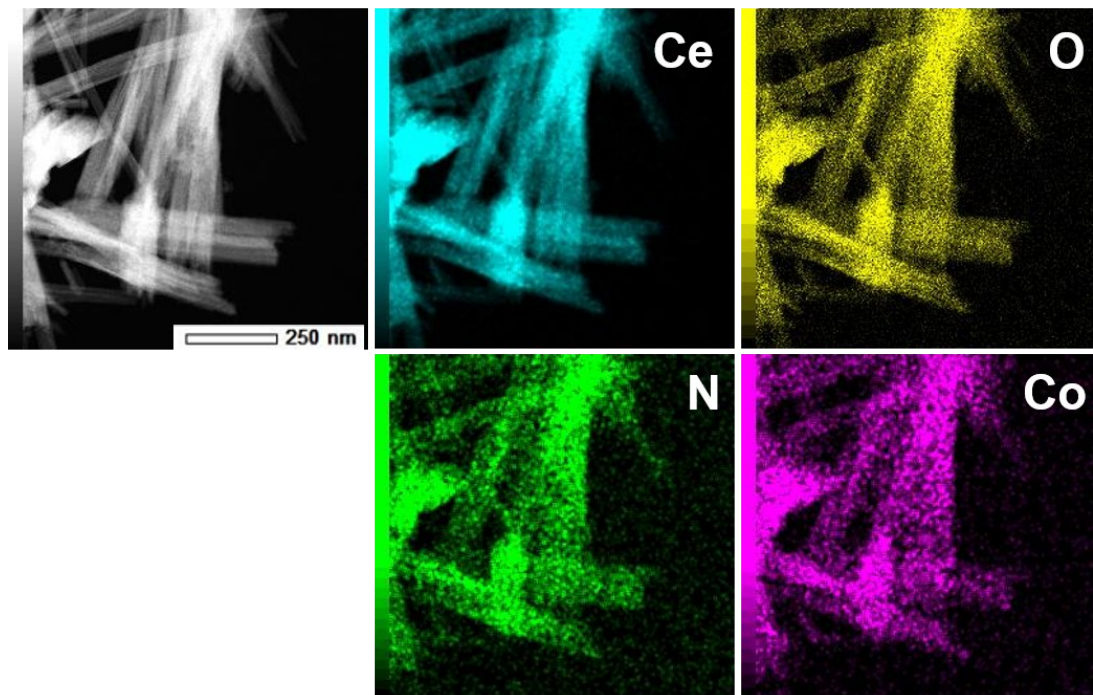


**Fig. S17** TEM-EDX mapping images of the  $\text{TCPP}@30\%\text{Co}_3\text{O}_4@\text{CeO}_2$  (1/30).

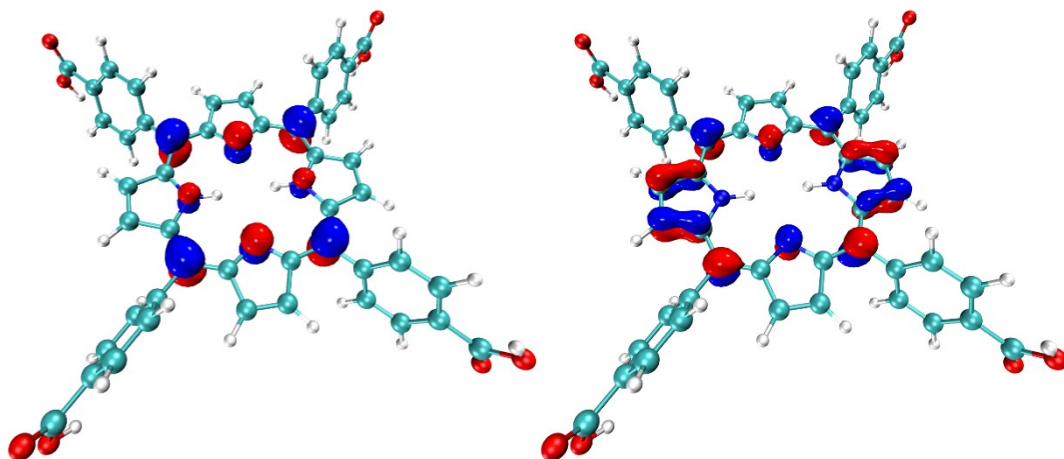


**Fig. S18** Molecular orbital (MO) of the H<sub>2</sub>TCPP, HOMO (left) and LUMO (right).

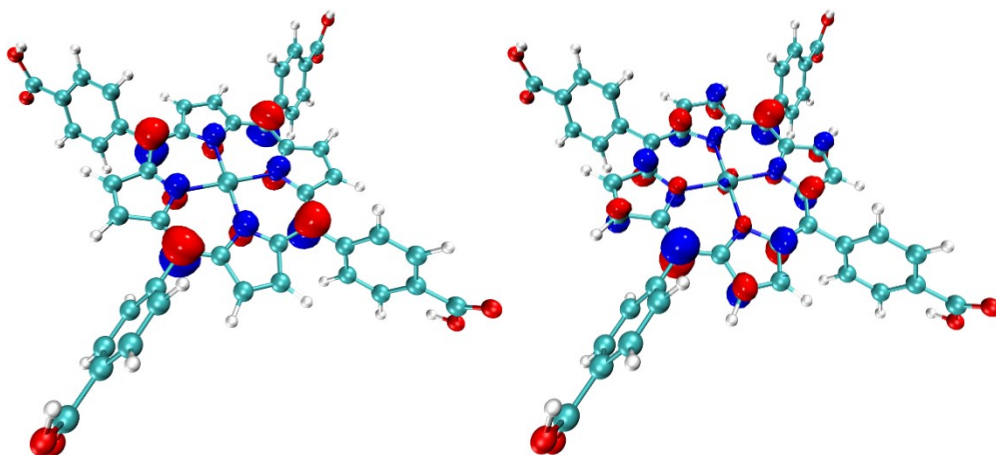


**Fig. S19** MO of the CoTCPP,  $\alpha$  HOMO (left) and  $\alpha$  LUMO (right).

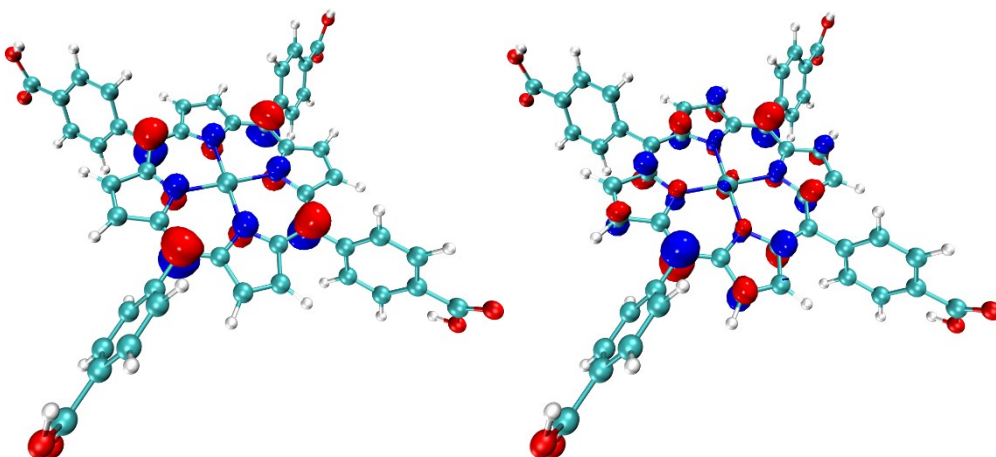


**Fig. S20** MO of the CoTCPP,  $\beta$  HOMO (left) and  $\beta$  LUMO (right).

**Table**

	<b>Chemical</b>	<b>Peak (eV)</b>	<b>AC%</b>
<b>O<sub>1</sub></b>	<b>Ce (IV)-O</b>	<b>529.57</b>	<b>27.05</b>
<b>O<sub>2</sub></b>	<b>Ce (III)-O</b>	<b>530.80</b>	<b>39.39</b>
<b>O<sub>3</sub></b>	<b>C=O</b>	<b>532.54</b>	<b>26.73</b>
<b>O<sub>4</sub></b>	<b>C-OH</b>	<b>534.14</b>	<b>6.83</b>

**Table S1** Fine peaks of O1s XPS before oxygen production test of the CoTCPP@CeO<sub>2</sub>=1:30.

	<b>Chemical</b>	<b>Peak (eV)</b>	<b>AC%</b>
<b>O<sub>1</sub></b>	<b>Ce (IV)-O</b>	<b>529.7</b>	<b>38.53</b>
<b>O<sub>2</sub></b>	<b>Ce (III)-O</b>	<b>530.59</b>	<b>14.58</b>
<b>O<sub>3</sub></b>	<b>C=O</b>	<b>532.1</b>	<b>37.24</b>
<b>O<sub>4</sub></b>	<b>C-OH</b>	<b>533.33</b>	<b>9.65</b>

**Table S2** Fine peaks of O1s XPS after oxygen production test of the CoTCPP@CeO<sub>2</sub>=1:30.

	<b>1:10</b>	<b>1:20</b>	<b>1:30</b>	<b>1:40</b>	<b>1:50</b>
<b>Oxygen vacancies (%)</b>	<b>39.77</b>	<b>35.9</b>	<b>39.39</b>	<b>48.25</b>	<b>45.70</b>
<b>Ce<sup>3+</sup>(%)</b>	<b>20.79</b>	<b>24.37</b>	<b>25.35</b>	<b>31.58</b>	<b>14.59</b>

**Table S3** Oxygen vacancies percentage composition of the CoTCPP@CeO<sub>2</sub>.

	<b>HOMO</b>	<b>LUMO</b>
<b>TCPP</b>	<b>-5.883938 eV</b>	<b>-3.198660 eV</b>
<b>CoTCPP (<math>\alpha</math>)</b>	<b>-5.933958 eV</b>	<b>-3.029727 eV</b>
<b>CoTCPP (<math>\beta</math>)</b>	<b>-5.934171 eV</b>	<b>-3.021372 eV</b>

**Table S4** Specific HOMO and LUMO level positions of TCPP and CoTCPP relative to vacuum levels.